Journal of the Brazilian Society of Mechanical Sciences and Engineering (2023) 45:167
https://doi.org/10.1007/s40430-023-04089-x

TECHNICAL PAPER

Optimization of NACA 4412 augmented with a gurney flap by using grey relational analysis

Ramazan Çakıroğlu[1] · H. Erdi Tanürün[2,3] · Adem Acır[3] · Furkan Üçgül[3] · Sena Olkun[3]

Received: 13 May 2022 / Accepted: 7 February 2023
© The Author(s), under exclusive licence to The Brazilian Society of Mechanical Sciences and Engineering 2023

Abstract

The gurney flap which has increased the lift coefficient at the trailing edge is used to improve the aerodynamic performance of the airfoil. In this study, the effect of the aerodynamic performance of baseline augmented with various dimensions of gurney flap (GF) structures was optimized by Taguchi method-based grey relational analysis (GRA) unlike previous works. Based on Taguchi's L_{16} orthogonal array method, the designs of the experiments were employed to optimize four control factors that were position (Δx), angle (α), thickness (Δt), and length (ΔL) of the GF on the airfoils. In aerodynamic studies based on GRA method, optimum parameters for α, ΔL, Δt, and Δx of GF were obtained as 75°, 1.5%c, 2%c, and 0%c. The degree of effect in aerodynamic performance was investigated by analysis of variance (ANOVA). The results show that the effect order of these four control factors was obtained as $\Delta x > \Delta h > \Delta t > \alpha$ which means that while Δx parameter with 37.62% has the strongest effect on the lift coefficient (C_L) and drag coefficient (C_D), α parameter with 3.06% has the lowest effect. The use of the GF model, which has the most optimal parameter, increased the efficiency (high C_L; low C_D) by 35.62% compared to the baseline in terms of GRA. In addition, empirical equations of the C_L and C_D on the airfoils were derived by regression analysis (RA). The values attained from empirical and numerical results (confirmation test) were highly compatible with each other.

Keywords Gurney flap · Aerodynamic performance · CFD · Grey relational analysis · Analysis of variance (ANOVA)

List of symbols

Δh	Length of Gurney Flap
Δt	Thickness of Gurney Flap
Δx	Position of Gurney Flap
A	Projection area of Airfoil
ANOVA	Analysis of Variance
AOA	Angle of Attack
c	Chord Length
C_D	Drag Coefficient
CFD	Computational Fluid Dynamics
C_L	Lift Coefficient
C_P	Critical Coefficient
$C\mu u$	Pressure Coefficient
Dof, ν_A	Degrees of Freedom
F_D	Drag Force
F_L	Lift Force
GRA	Grey Relational Grade
GRG	Grey Relational Analysis
GF	Gurney Flap
MS	Mean Sum of Squares
n	The Number of Observations
OA	Orthogonal Array
P	Static Pressure
RA	Regression Analysis
Re	Reynolds Number
R^2	The Percentage of Variation in the Response
S/N	Signal-to-Noise
SS, SS_A	Sequential Sum of Squares
SS_T	Total Sequential Sum of Squares
TKE	Turbulence Kinetic Energy
TI	Turbulence intensities
u	Friction Velocity at The Nearest Wall

Technical Editor: André Cavalieri.

✉ Ramazan Çakıroğlu
rcakiroglu@gazi.edu.tr

[1] Technical Sciences Vocational School, Gazi University, 06500 Ankara, Türkiye

[2] Department of Energy Systems Engineering, Elbistan Engineering Faculty, Kahramanmaraş Istiklal University, Kahramanmaraş, Türkiye

[3] Department of Energy Systems Engineering, Faculty of Technology, Gazi University, 06500 Ankara, Türkiye

Published online: 24 February 2023

v	The Friction Velocity of The Fluid
V	Velocity
VAWT	Vertical axis wind turbine
V_e	Variance Error
x, y, z	Cartesian Coordinates
y^+	Normalized Wall-Normal Coordinate
y	The Observed Data
α	Angle of Gurney Flap
ρ	Density

1 Introduction

With the depletion of fossil fuels and the irreversible damage to the nature, the world requires new energy sources more than ever [1]. Therefore, scientists aim to optimize and improve renewable energy technologies like wind turbines and photovoltaic technologies. There are several parameters that affect the performance of the wind turbine, the leading of which is blade aerodynamics. Many studies have been carried out in the literature in recent years to improve the airfoil aerodynamics and improve its performance. Aerodynamic performance was investigated by optimizing the geometry of the airfoil with various vortex generators, such as tubercle [2, 3], dimple [4–6], and flap. The vortex generator was used extensively to provide passive flow control as well as to improve the aerodynamic performance of the airfoils. Although there are various types of flaps, the gurney flap (GF) is one of the most widely applied flap models in airfoils due to its high lift effect. The GF, integrated as a small indentation in the trailing edge of the airfoil, improved lift by increasing the effective circulation depending on the Kutta conditions. However, on the other hand, GF also increases the drag due to prevent the flow. Therefore, the determination of the GF geometry to be integrated into the blades of wind turbines is carried out as a result of a detailed examination. Liebeck brought the first investigation into the literature and made experimental research on the airfoils with GF [7]. Storms et al. experimentally investigated the effect of different lengths and positions of GF on the NACA 4412 airfoils. It was determined that the GF improved lift coefficient (C_L) by 31.5% at Reynolds number (Re) under 2×10^6[8]. Li et al. studied the effects of attack angles and locations of the GF on performance under 2.1×10^6 conditions in the NACA 0012 airfoil model, and their results revealed that all placements improved the C_L, and the best performance was gotten by the 45° GF from all flap experiments [9]. Meyer et al. revealed various modifications of the created GF using slots and holes at $Re=1\times10^6$ that can decrease the drag coefficient [10]. Shukla et al. numerically investigated the profile modifications of GF, dimple, and both on 4 different symmetrical NACA blades using the Spalart–Allmaras turbulence model method in CFD application. In the results, it was determined that p GF showed better results than dimple in all conditions [4].

Zhu et al. conducted a numerical investigation to improve efficiency on straight-bladed vertical axis wind turbine (VAWT) with integrated of GF and dimple-GF using NACA 0012 airfoil at $Re=5{,}28\times10^4$. When the results were analyzed, the model with only the GF improved the power coefficient by 10.9% compared to the bare turbine and by 17.9% with the addition of both dimple and GF [11]. Zhang et al. numerically observed that the GF increased the thrust and torque values at $Re=2.5–3.5\times10^6$ on the NACA 63,424 and NACA 63,421 airfoils. It was also observed that the GF improved the power coefficient by 21% [12]. Fatahian et al. numerically investigated the aerodynamic performance of the NACA 0012 airfoil using jet locations, velocity ratios, jet angles, and flaps at $Re=5\times10^5$ using SST k-ω turbulence model. In the results, they obtained that the lift coefficient of the optimal airfoil increased by approximately 60% and the drag coefficient decreased by 82% [13]. In this study of Kumar and Samad, they numerically observed that the GF increased the load on the NACA 0015 airfoil at various Re numbers using SST k-ω turbulence model, and the torque produced from the airfoil has increased. Stall was improved at gurney lengths greater than 1.5%c [14]. Saenz-Aguirre et al. numerically investigated significant increase in the energy produced at $Re=2\times10^6$ when the artificial neural network-based gurney flap was integrated into the wind turbine with numerous airfoil models. [15]. Yang et al. experimentally examined aerodynamic performance with various GF configurations on the DTU-LN221 airfoil model with $Re=1.5\times10^6$ at three different turbulence intensities (TIs) between 0.2% and 19%. In the results, they found that the most effective C_L was improved up to 13.5% with low turbulence intensity. Additionally, the effect of the GF decreased after the stall angle [16]. Fatahian et al. numerically investigated the effect of different hinge positions on the aerodynamic performance of the NACA 0012 airfoil at $Re=5\times105$ using SST k-ω turbulence model at $Re=5\times10^5$ using SST k-ω turbulence model. The results showed that the optimal hinge position increased significantly C_L/C_D [17]. Ni et al. found that the gurney flap added to the outer side of the wind turbine blade (NACA 0018), could significantly improve torque performance at $TSR\leq2.51$ in VAWT [18]. Zhu et al. numerically examined that the optimal position of the gurney flap on NACA 0021 improved the aerodynamic performance by 21.62% in VAWT and also increased the blade tangential force in the upstream region [19]. Sun et al. working with NACA 0012 numerically investigated that as the gurney flap height increases at $Re=2\times10^6$ with Spalart–Allmaras turbulence model; the tail vortex increases, while the average power increase is limited [20].

Since the GF has a major impact on blade aerodynamics, various investigations have been performed in the literature

using different GF geometry parameters. However, as the effects of various parameters are so difficult to examine simultaneously, those parameters have been examined individually or with limited parameters in pairs and triples in literature. Authors have not found a study investigating the aerodynamic performance by collecting all the parameters of the GF under a certain algorithm in the literature. Therefore, using optimization methods for cost and schedule management of a large number of difficult-to-control parameters creates an efficient process.

In the literature, the gurney flap profile has been studied intensively in recent years due to its positive effect on aerodynamic performance. Gurney flap (GF) increases the lift coefficient (C_L) at the trailing edge. On the other hand, the lift force increases while the drag force also increases. However, a study given in which optimal parameters both C_L and C_D were obtained by using an optimization method of the parameters forming the geometry of the gurney flap has not been found in the literature. The aim of this study is numerically evaluating the effect of simultaneous GF parameters on the aerodynamic performance of the NACA 4412 airfoil at 0° angle of attack, Taguchi based on grey relational analysis approach (GRA), which is an optimization model. Because the GF increases both C_L and C_D, effective GF geometry is extremely important to determine the optimal aerodynamic efficiency (C_L/C_D). In order to obtain optimal C_L/Cd, the grey relational grade (γ_1) value must be high in the GRA approach. γ_1 is defined as low C_D and high C_L. In this manner, optimal flap geometry was obtained with much less numerical analysis compared to the conventional method. Numerical studies were carried out as three-dimensional simulations of 16 different algorithms consisting of 4 different variables for each of the 4 parameters (factors): position, angle, length, and thickness. The impact levels of the factors were performed by ANOVA analysis, and empirical equations were procured in regression analysis (RA). Besides, the model obtained with the optimal GF configuration was compared with the baseline in terms of flow characteristic.

2 Material method

2.1 Governing equations and performance parameters

3D CFD simulations were carried out with the commercial solver ANSYS-fluent software program. The discretization was performed by the COUPLED algorithm for pressure–velocity coupling along with second-order and second-order upwind schemes by under-relaxation factors. The inlet boundary conditions were determined as $\mathrm{Re} = 3.6 \times 10^4$ based on velocity of inlet flow $V_\infty = 10$ m/s, air density was 1.225 kg/m^3, and dynamic viscosity of air was 1.7894×10^{-5} N.s/m^2. Pressure outlet gauge pressure was "0" Pa. The scale residual was applied as 5×10^{-5} throughout all numerical study.

The Reynolds-averaged Navier–Stokes (RANS) equations were chosen as the flow field's governing equations. In RANS, the flow properties are disintegrated into their mean and fluctuating components and integration over time (i.e., time-averaging) is performed. The governing equations for RANS model are given in the following [21].

$$\frac{\partial \overline{u_l}}{\partial \overline{u_j}} = 0, \tag{1}$$

and

$$\overline{u}_j \frac{\partial \overline{u_l}}{\partial \overline{u_j}} = -\frac{1}{\rho}\frac{\partial \overline{p}}{\partial x_i} + \nu \frac{\partial^2 \overline{u_l}}{\partial x_{j^2}} - \overline{u_j \frac{\partial u_i}{\partial x_j}} \tag{2}$$

where ν denotes the kinematic viscosity of the air, q the density of air, ρ the pressure, ui, and $-\overline{u_i u_j}$ the mean velocity and the Reynolds stress, respectively.

In this study, the k-ε realizable turbulence model, which is widely used in aerodynamic studies in the literature, derived from the standard k-ε model, was used in this study [22, 23]. This model contains a new transport equation for the turbulent dissipation rate. Moreover, the critical coefficient of the model, $C\mu u$, is expressed as a function of mean flow and turbulence properties, rather than assumed to be constant as in the standard model [24, 25]. The transport equations for k-ε and k-ε Realizable models are presented in the following.

$$\frac{\partial}{\partial t}(\rho k) + \frac{\partial}{\partial x_j}\left(\rho k u_j\right) = \frac{\partial}{\partial x_j}\left[\left(\mu + \frac{\mu_t}{\sigma_k}\right)\frac{\partial_k}{\partial x_j}\right] + G_k + G_b - \rho\varepsilon - Y_m + S_k \tag{3}$$

and,

$$\frac{\partial}{\partial t}(\rho \varepsilon) + \frac{\partial}{\partial x_j}\left(\rho \varepsilon u_j\right) = \frac{\partial}{\partial x_j}\left[\left(\mu + \frac{\mu_t}{\sigma_\varepsilon}\right)\frac{\partial_\varepsilon}{\partial x_j}\right] + \rho C_1 S\varepsilon - \rho C_2 \frac{\varepsilon^2}{k + \sqrt{\upsilon\varepsilon}} + C_{1\varepsilon}\frac{\varepsilon}{k} C_3 G_b + S_\varepsilon \tag{4}$$

where,

$$C_1 = max\left[0, 43\frac{\eta}{\eta + 5}\right] \text{and}, \eta = S\frac{k}{\varepsilon} \tag{5}$$

where Y_m depicts the contribution of the fluctuating dilatation in compressible turbulence to the overall dissipation rate, and $C_{1\varepsilon}$, $C_{2\varepsilon}$, and $C_{3\varepsilon}$ are constants. G_k denotes the generation of turbulence kinetic energy due to the mean velocity gradients. G_b represents the generation of turbulence kinetic energy due to buoyancy. The turbulent Prandtl numbers for k

and ε are, respectively, σ_k and σ_ε. User-defined source terms include S_k and S_ε [26].

The aerodynamic performance of an airfoil is described by several key characteristics. While the force created by the relative wind speed perpendicular to the airfoil is the lift force, the force parallel to the airfoil is expressed as the drag force. Lift (C_L) and drag coefficient (C_D) were derived from lift and drag force in Eqs.(6 and 7) [27].

$$C_L = \frac{F_L}{\frac{1}{2}\rho V^2 A} \tag{6}$$

$$C_D = \frac{F_D}{\frac{1}{2}\rho V^2 A} \tag{7}$$

where ρ denotes density, and v represents velocity, while A is the airfoil projection area. F_L and F_D represent lift and drag force, respectively.

2.2 Design of numerical tests

In this study, the commercial program MINITAB 20 was used, and the effects of GF parameters, such as angle (α), length (Δh), thickness (Δt), and position percentage (Δx), on the coefficients of lift and drag were investigated. The specified factors with symbols and their coded levels are presented in Table 1. Although there are various parameters of the GF on airfoil that affect the C_L and C_D, the parameters selected in Table 1 are the most effective ones. The numerical experiment layout for the flap design parameters consisted of the L_{16} orthogonal array matrix using factors and levels is illustrated in Table 2.

2.3 Grey relational analysis methods

The fundamental goal in the GRA procedure is to convert the performance of each alternative into a comparison sequence expressed as grey relational generating. Then an ideal sequence is created, and the grey relational coefficient between this ideal sequence and all other comparability arrays is obtained. Depending on the grey relational coefficients, between every comparability and the ideal target arrays grey relational grade is calculated. Among the comparability arrays, the sequence that produces the best grey relational grade with the ideal target array is determined as the optimal alternative sequence [28]. The schematic view of the grey relational analysis is given in Fig. 1. The GF has a significant effect on the aerodynamic performance of the blade. GF geometry comprises various parameters. While every parameter has different variables, determining the optimal parameters with conventional methods becomes difficult. The four factors selected for this study have four variables. Classical methods can only determine the optimal flap geometry as a result of 256 numerical studies. The optimal GF parameters, across the other side, are obtained through 16 numerical experiments using the GRA optimization method.

Optimization methods such as the Taguchi Method and GRA are used in a variety of applications. The Taguchi-based GRA method differs from others due to the fact that it can optimize two or more data sets at the same time, and it was used in this study to determine optimal parameters for high C_L and low C_D.

The GRA method's first application step in all is normalizing output data parameters. As seen in Eqs. 8–10, there are three normalization methods: the larger the better, the nominal the better, and the smaller the better [29, 30].

Larger the better normalization is shown in Eq. 8.

$$x_i(k) = \frac{x_i^0(k) - \min x_i^0(k)}{\max x_i^0 - \min x_i^0(k)} \tag{8}$$

Table 1 Gurney flap geometry parameters and their level

Symbol	Factor	Levels			
		1	2	3	4
A	Angle (α)	90°	75°	60°	45°
B	Length (Δh)	1.5%c	3%c	4.5%c	6%c
C	Thickness (Δt)	1%c	2%c	3%c	4%c
D	Position (Δx)	0%c	6%c	12%c	18%c

Table 2 L_{16} orthogonal array

Test number	Angle (α) A	Length (Δh) B	Thickness (Δt) C	Position (Δx) D
1	1	1	1	1
2	1	2	2	2
3	1	3	3	3
4	1	4	4	4
5	2	1	2	3
6	2	2	1	4
7	2	3	4	1
8	2	4	3	2
9	3	1	3	4
10	3	2	4	3
11	3	3	1	2
12	3	4	2	1
13	4	1	4	2
14	4	2	3	1
15	4	3	2	4
16	4	4	1	3

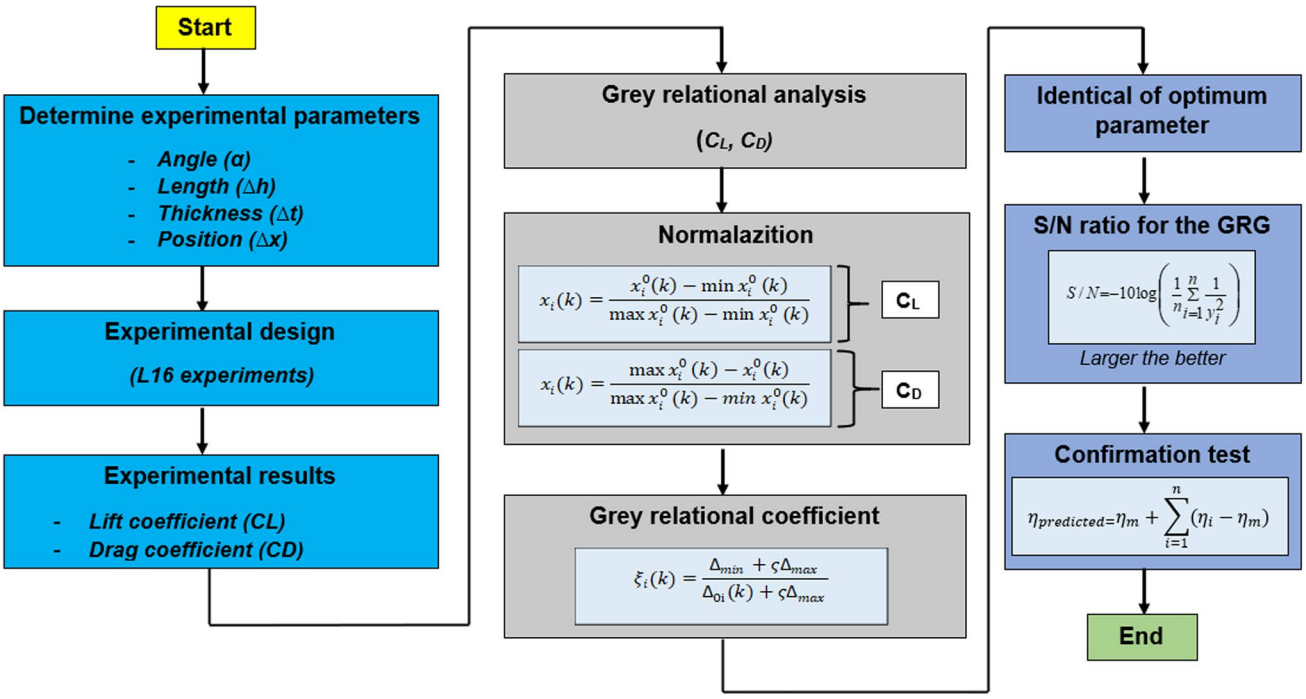


Fig. 1 Method of grey relational analysis

$x_i^0(k)$ original value at i series k. row, x_i (k) after normalization value at i series k. row, min $x_i^0(k)$ is the minimum value at i series, and max $x_i^0(k)$ is the maximum value at i series.

The smaller the better normalization is shown in Eq. (9).

$$x_i(k) = \frac{\max x_i^0(k) - x_i^0(k)}{\max x_i^0 - \min x_i^0(k)} \tag{9}$$

The nominal the better normalization is shown in Eq. (10).

$$x_i(k) = 1 - \frac{x_i^0(k) - x^0)}{\max x_i^0 - x^0)} \tag{10}$$

x^0 denotes the desired ideal value.

Next step of the GRA method is defining m series to compare with x^0 in Eq. (11).

$$x_i = \left(x_i(1), x_i(2), x_i(3), \ldots\ldots, x_i(n)\right) i = 1, 2, \ldots, m \tag{11}$$

k denotes the k. row in the series at n length. $\varepsilon(x_0(k), x_i(k))$ is grey relational coefficient at k. point and given in Eqs. (12–15).

$$\varepsilon\left(x_0(k), x_i(k)\right) = \frac{\Delta\min + \xi\Delta\max}{\Delta_{0i}(k) + \xi\Delta\max} \tag{12}$$

$$\Delta_{0i}(k) = \left|x_0(k) - x_j(k)\right| \tag{13}$$

$$\Delta_{min} = \min_j \min_k \left|x_0(k) - x_j(k)\right| \tag{14}$$

$$\Delta_{max} = \max_j \max_k \left|x_0(k) - x_j(k)\right| \tag{15}$$

$\xi \in$ is a value between (0,1). $j = 1,2,\ldots,m$; $k = 1,2,\ldots,n$. ξ function arranges the difference between Δ_{0i} and Δ_{max}. Studies show the ξ function does not affect the post-grey relation degree order [31].

Eq. (16) provides grey relational degree calculations.

$$\gamma\left(x_0, x_i\right) = \frac{1}{n}\sum_{k=1}^{n} \varepsilon(x_0(k), x_i(k)) \tag{16}$$

$\gamma\left(x_0, x_i\right)$ is a measure of geometric similarity between x_i and x_0 reference series in a grey system. Size of the grey relational degree shows a strong relationship between x_i and x_0. If the series being compared are the same, the grey relationship degree is "1". The grey relational degree demonstrates how the compared series is similar to the reference series.

If the weights of all parameters are given, the grey relationship degree is found by multiplying the grey correlation coefficient of the parameters and the weight value of the importance degree of the parameters. It is calculated as Eq. 17.

$$\gamma\left(x_0, x_i\right) = \frac{1}{n}\sum_{k=1}^{n} \varepsilon(x_0(k), x_i(k) * (W_i(k))) \tag{17}$$

The GRA utilizes the signal-to-noise (S/N) ratio for the desired quality characteristic and the S/N ratio differs according to any objective function, i.e., each characteristic value. Therefore, the S/N ratio is used as a measurable value instead of the standard deviation [32]. The larger the better characteristic is used, and the corresponding in Eq. (18) is provided below.

The larger the better characteristics:

$$\frac{S}{N} = -10\log\frac{1}{n}(\sum 1/y^2) \tag{18}$$

To be more specific, n is the number of observations, and y is the observed data. The unit for the S/N ratio is decibels (dB), and for each type of characteristic, with the above S/N ratio transformation, the increase in the S/N ratio improves the result. The numerical experiment results and relevant S/N ratios are exhibited in the results section.

3 Result and discussion

3.1 Geometry

NACA 4412 model, a 4-digit airfoil model which is widely used in the aerodynamic studies [33–38]. In addition, chord (c) and spanwise (ω) values were assigned as 66.6 and 200 mm, respectively, with the model aspect ratio of 3. In Fig. 2, the geometric features of the baseline, airfoil with GF and detail GF were shown. The values of the four factors that create the GF geometry were expressed in terms of chord length (c).

Computational domain and boundary condition rates are shown in Fig. 3. C-type computational domain was used due to its ability to provide the fluid to reach the blade surface perpendicularly [24, 39]. Besides, the fact that the boundary conditions were large enough ensured that the results obtained from the study were independent of the boundary conditions. Therefore, inlet, outlet, and symmetry boundary conditions are assigned as 25c, 25c, and 50c, respectively.

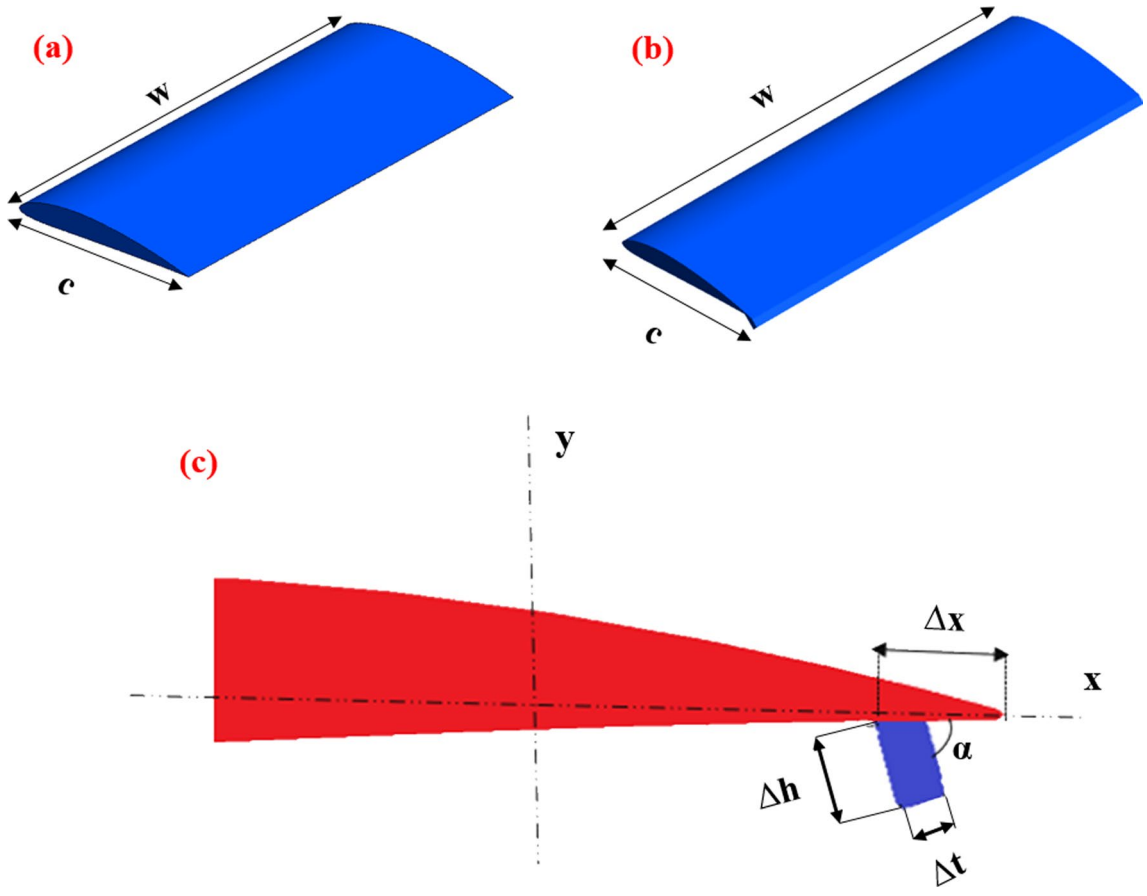


Fig. 2 Isometric geometry of **a** baseline **b** $\alpha = 75°$; $\Delta h = 6\%c$; $\Delta t = 3\%c$; $\Delta x = 6\%c$ (see Table 3: test no 8) detail view of flap geometry (NACA 4412 airfoil)

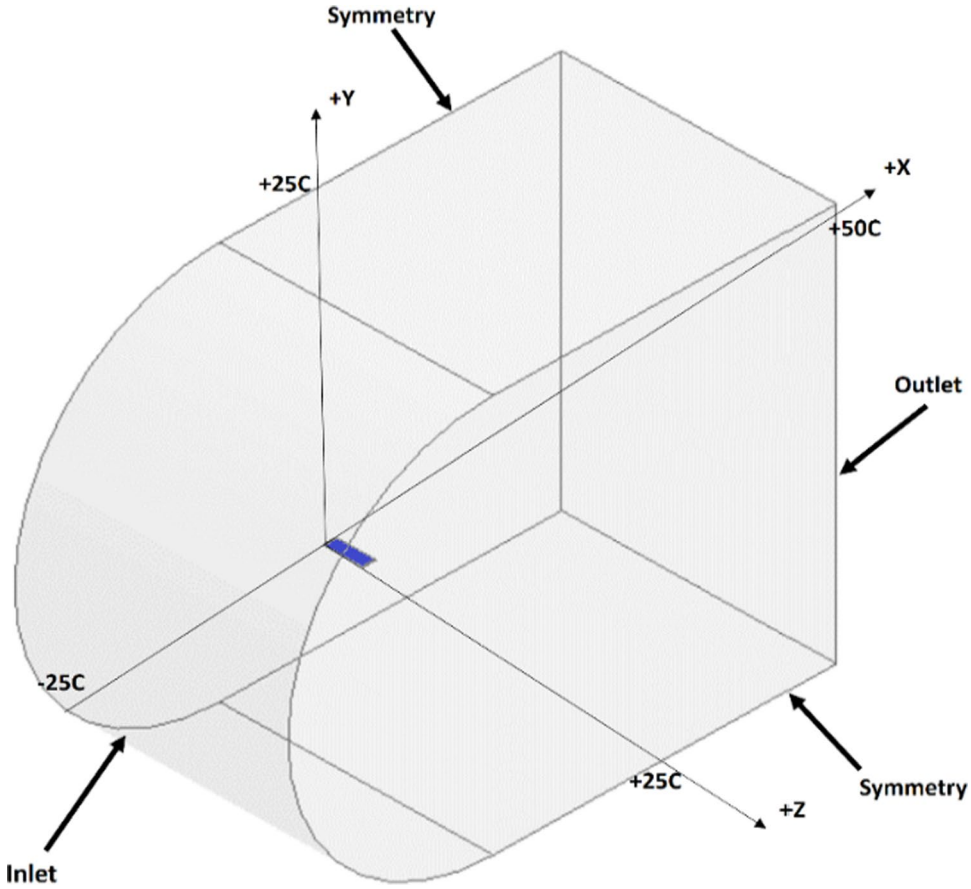


Fig. 3 Computational domain isometric view

3.2 Grid dependence study

The computational grid is crucial for numerical study accuracy. Creating responsible grids lowers computational costs and assures that the accurate result is reached. Mesh sizes are not the same in every region of the computational domain. The mesh size gradually decreases from the blade surface to the other parts of the enclosure so that the number of meshes around the blade has more density.

Due to asymmetrical airfoil geometry and the complex structure of the gurney flap, the grid distortions increase. Therefore, the unstructured triangular meshing method, which commonly applied in literature studies [40, 41], is preferred. In this paper, C_L in nine different mesh models were produced among 2.3 and 13.7×10^5 mesh range at a 12.5 angle of attack, as seen in Fig. 4. The 12.5 angles of attack was set because of its close to the stall angle. Since the error rate of the results achieved from the change of the mesh number procured after 1,186,378 cells is 0.5%, accepted as a reasonable mesh number. The grid distribution of the computational domain with 1,186,378 cells is exhibited in Fig. 5.

While improving mesh, creating boundary layer regions around the critical areas of the design is essential. Based on theoretical derivations and experimental explorations, the boundary layers are classified into viscous sub-layer ($y^+ \leq 5$), buffer layer ($5 < y^+ \leq 30$), log-law region ($30 < y^+ \leq 500$), and outer layer [42]. The value of y^+ is defined as in Eq. (19). In order to predict the aerodynamic performance of the airfoil, it is necessary to obtain a viscous sub-layer in order to accurately express the variations in the flow characteristics in the transition from the laminar zone to the turbulent zone and to prevent distortions on the airfoil surface. In this study, 12 inflation layers in the form of a 0.014 mm first layer thickness with a growth rate of 1.09 were utilized. In Fig. 6, the y^+ of the baseline is lower than the obtained optimum model ($\alpha = 75°$; $\Delta h = 1.5\%$c; $\Delta t = 2\%$c; $\Delta x = 0\%$c). However, it was determined that both the all surface of baseline and obtained optimum model were between 0–1 in terms of y^+. In addition, y^+ of other model's entire surface was attained as less than 1.

$$y^+ = \frac{u * y}{v}, \tag{19}$$

where u is the friction velocity at the nearest wall, y is the distance to the nearest wall, and v is the local kinematic viscosity of the fluid [43, 44].

In Table 3, another way to check for responsible grid cells is to examine the element quality, orthogonal quality and skewness rates of the grid structure. The skewness

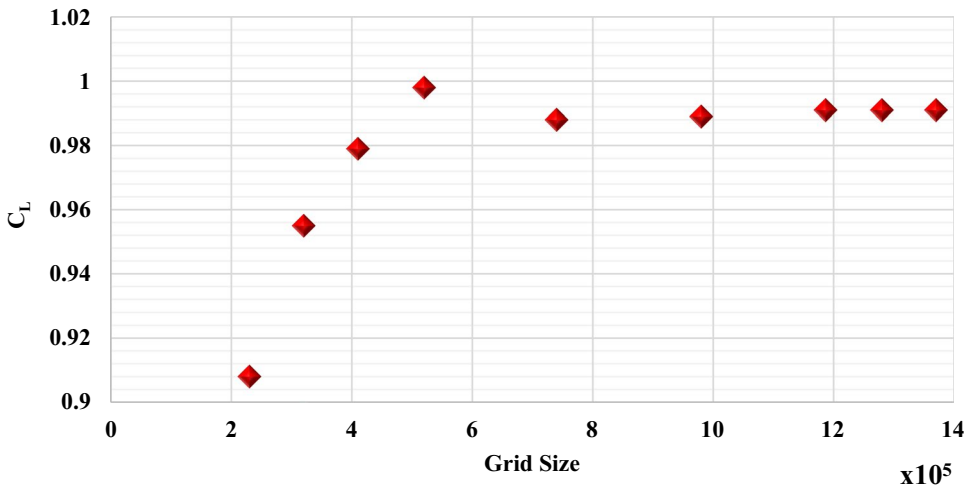


Fig. 4 C_L values of the baseline model at 12.5° angle of attack

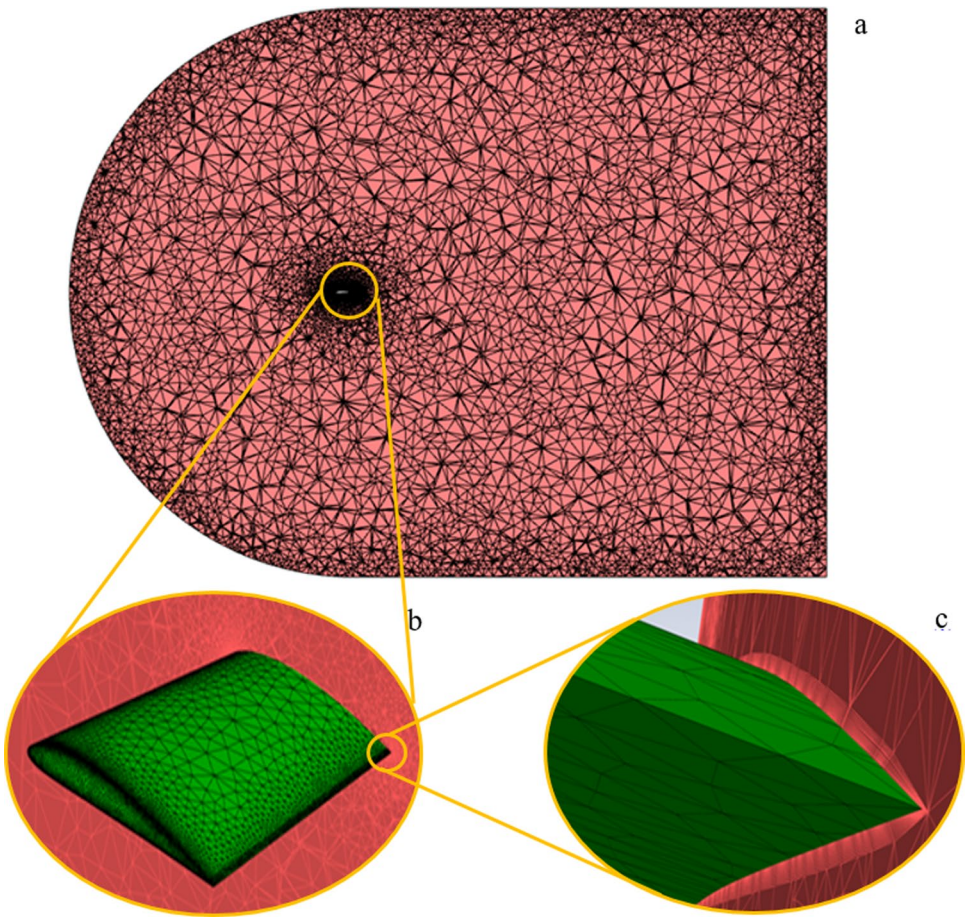


Fig. 5 Grid structure on **a** C-type domain **b** baseline isometric view, **c** the inflation layer of the baseline surface at 11.8×10^5 mesh number

range should be between 0 and 1, while closer to 0 is better, and the element and orthogonal qualities range should be between 0 and 1, and closer to 1 is better. Therefore, the values obtained for both skewness and orthogonal quality are within the range that is acceptable for studies.

3.3 Validation

The 3D analysis of the vortex type was yielded more realistic results than the 2D operation airfoil. However, even if the analysis is 3D in the study, it is extremely important for

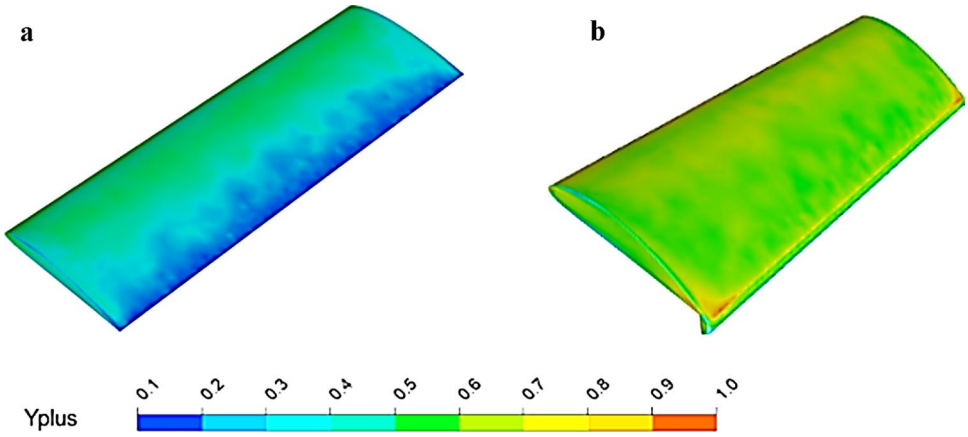


Fig. 6 y^+ distribution around of **a** baseline **b** obtained optimum parameters (α = 75°; Δh = 1.5%c; Δt = 2%c; Δx = 0%c) at 0° attack of angle

Table 3 Mesh quality

	Grid number	Element quality	Orthogonal quality	Skewness
Baseline	1,186,378	0.8072	0.8256	0.1746

the reliability of the study to be verified with the literature. In light of this information, as seen in Fig. 7, the baseline was compared with studies [45–49] in terms of C_L x α. The majority of the studies determined for verification were paid attention to be 4-digit, asymmetric and similar Re values in order not to be deceptive. When Fig. 7 is examined, it has been observed that the present study and studies with similar Re in the literature, especially Jukes et al. [47], show a similar behavior. Compared to the literature, the small differences in stall and slope are due to the different asymmetric values and aspect ratio of the NACA blades in the study, as well as the error rate differences in the experimental studies in the literature. However, this difference is acceptable in the literature, considering the similar slope and reasonable C_L.

3.4 Application of the grey relational analysis

In the first instance, the numerical experiment was carried out for NACA 4412 without the GF attached. C_L, C_D and γ_1 at 0° attack angle for baseline (NACA 4412 without flap) were 0.223, 0.039 and 0.5139, respectively. After the C_L and C_D of the baseline were obtained, the factors and levels in Table 1 were converted to the design parameters in Table 2. All the numerical analyses were carried out at 0° angle of attack, and the results of the GRA data generated based on numerical analyzes are demonstrated in Table 4. High γ_1 indicates strong correlation between normalization value and

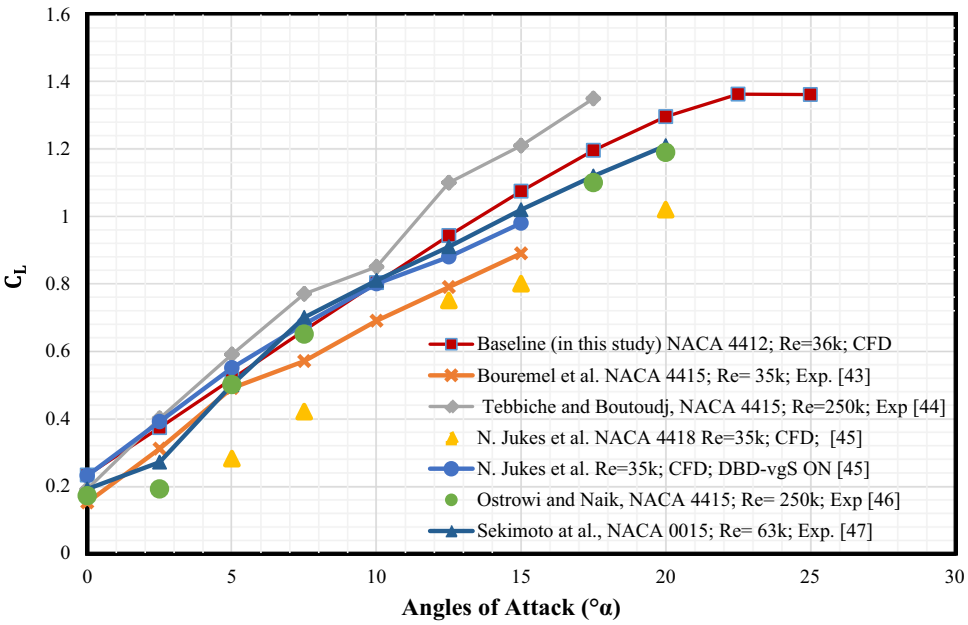


Fig. 7 The C_L verification at various angles of attack

Table 4 Numerical results and S/N ratios for lift coefficient (C_L) and drag coefficient (C_D)

Exp. No	Numerical results		Normalized values		Grey relational coefficients		Grey relational grade, γ_1	Signal-to-noise (S/N) ratio	Order
	C_L	C_D	C_L	C_D	C_L	C_D			
1	0.39	0.06	0.223	0.986	0.392	0.973	0.682	−3.31865	1
2	0.41	0.07	0.276	0.764	0.409	0.680	0.544	−5.28740	6
3	0.44	0.09	0.351	0.531	0.435	0.516	0.476	−6.45529	15
4	0.47	0.10	0.400	0.308	0.455	0.419	0.437	−7.18928	16
5	0.29	0.06	0.000	1.000	0.333	1.000	0.667	−3.52183	2
6	0.34	0.07	0.125	0.773	0.364	0.688	0.526	−5.58369	7
7	0.61	0.11	0.723	0.264	0.643	0.404	0.524	−5.61483	8
8	0.62	0.12	0.750	0.083	0.667	0.353	0.510	−5.84894	11
9	0.31	0.07	0.056	0.840	0.346	0.758	0.552	−5.15923	5
10	0.49	0.09	0.442	0.463	0.472	0.482	0.477	−6.42242	14
11	0.54	0.09	0.575	0.470	0.541	0.486	0.513	−5.79560	10
12	0.73	0.12	1.000	0.000	1.000	0.333	0.667	−3.52183	2
13	0.47	0.08	0.414	0.641	0.460	0.582	0.521	−5.66062	9
14	0.65	0.10	0.812	0.398	0.727	0.454	0.590	−4.57739	4
15	0.46	0.09	0.386	0.512	0.449	0.506	0.477	−6.42106	13
16	0.52	0.09	0.518	0.470	0.509	0.486	0.497	−6.06476	12

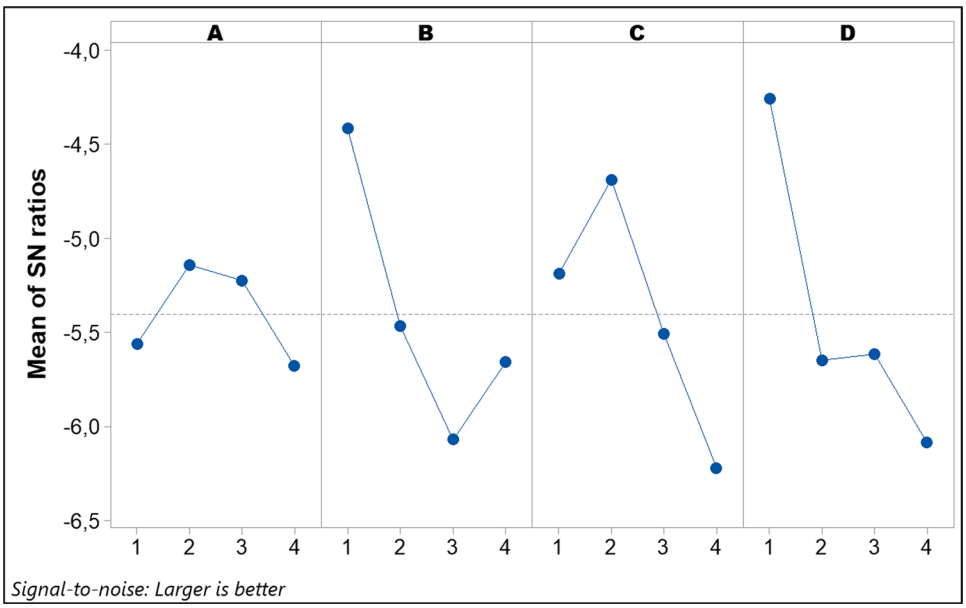


Fig. 8 Mean of S/N ratio for each level of factor

Table 5 Response table for signal-to-noise (S/N) ratios (larger is better)

Parameters	Level 1	Level 2	Level 3	Level 4	Delta
A: Angle (α)	0.5348	***0.5566***	0.5523	0.5216	0.0350
B: Length (Δh)	***0.6056***	0.5344	0.4975	0.5278	0.1081
C: Thickness (Δt)	0.5547	***0.5887***	0.5321	0.4899	0.0988
D: Position (Δx)	***0.6159***	0.5221	0.5293	0.4981	0.1177
	Total average value of the $\gamma_1 = 0.5917$				

Bold values indicate the levels of the optimum parameter obtained as a result of the optimization (A2B1C2D1)

the numerically result. The higher correlation demonstrates that GF geometry parameters have approached to optimal level. In Table 4, the γ_1 of baseline and experimental number "1" with the highest optimal parameters in terms of aerodynamic performance are compared, and it is observed that the γ_1 of no1 is 32.71% higher.

Figure 8 illustrates that the analysis of all levels of each factor was performed via the S/N ratio as a graph derived from Table 5. Flap parameters levels with the maximum performance could be obtained at the peaks of the stated S/N graph. In Fig. 8, the peak points at each level constituting the A2B1C2D1 levels were optimum model ($\alpha = 75°$; $\Delta h = 1.5\%$c; $\Delta t = 2\%$c; $\Delta x = 0\%$c), respectively. However, it was determined that A2B1C2D1 was not present in the design parameters in Table 2. Therefore, numerical analysis must be performed by creating a flap geometry obtained from optimum model.

The comparison of the predicted C_L with the actual C_L using the novel optimal flap parameters (A2B1C2D1) is illustrated in Table 6. Improvement of γ_1 ratio from baseline ($\gamma_1 = 0.5139$) and the initial flap ($\gamma_1 = 0.5139$) parameters to obtained optimal parameter flap ($\gamma_1 = 0.697$) was 35.62% and 19.9%. For this reason, it was an inevitable result that there was a remarkable increase in the aerodynamic performance due to flap optimization through GRA approach. In addition, it was observed that the accuracy of the GRA approach was quite reliable.

Table 6 Result of confirmation tests for the lift coefficient (C_L) and drag coefficient (C_D)

	Initial parameters	Optimum parameters	
		Prediction	Experiment
Level	*A1-B2-C3-D3*	*A2-B1-C2-D1*	*A2-B1-C2-D1*
γ_1	0.581	0.742761	0.697
S/N ratio (dB)	−4.7164	−2.2955	−3.7819
The improvement in $\gamma_1 = 0.116$ dB			
The percentage improvement in $\gamma_1 = 19.9\%$			

3.5 Analysis of variance (ANOVA) for GFs

Until this section, it was aimed to determine the most suitable set of design parameters to obtain the optimal aerodynamic performance. However, the order and extent of the effect of the design factors on the numerical results could not be determined. Analysis of variance (ANOVA) is a method that is used for determining factors and is a widely used method to identify important parameters and measure their effects [32]. Consequently, with the ANOVA, contribution quantities and ranks of the parameters were determined by using the percent contribution ratio (PCR) equation as presented in Eq. (20) [50].

$$\mathrm{PCR} = \left(\frac{\mathrm{SS}_A - \left(V_e\right)\left(\nu_A\right)}{\mathrm{SS}_T} \right) \mathrm{x}100 \tag{20}$$

Dof, SS, and MS subordinates represent degrees of freedom, sequential sum of squares, and mean sum of squares, respectively, according to Table 7 [50]. The F-test indicates specific levels of confidence, which assist in understanding the significance levels. Besides this, the P-value and F-test have a significant impact on the performance of the analysis results. Among the four factors, with 37.62%, factor D, which expresses the position of the flap, contributed majorly to aerodynamic performance, as seen in Table 7. B and C's contributions were 29.52% and 24.32% respectively, and these two factors' contributions were behind factor D, as a percentage. Factor A, which was the thickness of the flap, was the factor that had the least impact, with 3.06%. Essentially, in Table 7 illustrates that the position of the flap has the most significant effects on the aerodynamic performance as a factor, while the angle has a less significant role. Furthermore, the residual error rate was procured as 5.48%, which was an accepted error rate in the literature.

3.6 Regression analysis

Regression analysis is a method based on statistical basis. Regression analysis is an analytical method used to

Table 7 Results of ANOVA for aerodynamic performance

Parameter	Degree of freedom	Sum of squares	Mean of squares	*F*	*P*	PCR (%)
A: Angle (α)	3	0.8099	0.26996	3.79	0.151	3.06
B: Length (Δh)	3	5.9658	1.98859	27.91	0.011	29.52
C: Thickness (Δt)	3	4.9527	1.6509	23.17	0.014	24.32
D: Position (Δx)	3	7.5431	2.51436	23.17	0.014	37.62
Error	3	0.2137	0.07124			5.48
Total	15	19.4851				

DoF Degrees of freedom, *SS* Sequential sum of squares, *MS* Mean sum of squares

understand the correlation between input and output values in the analysis. As seen in Eq. (21), a linear regression is obtained in which each independent variable is related to the dependent variable [51].

$$y = \beta_0 + \beta_1 x_1 + \beta_2 x_2 + \cdots + \beta_n x_n + e \quad (21)$$

where x and y are, respectively, the input and output variable, β_0 is the intersection point, e is the remaining error.

The correlations among α, Δh, Δt, and Δx were obtained by regression analysis. With the regression analysis, the effect of factors on the quality characteristic of NACA 4412 with GF was attained in Eqs. (21–22). The C_L and C_D equation based on flap geometry were derived by simple linear regression analysis using MINITAB 20, and Eqs. (22–23) have been obtained as below:

$$C_L = 0.253 + 0.0496 * \mathrm{A} + 152 * \mathrm{B} + 21.4 * \mathrm{C} - 18.3 * \mathrm{D} \quad (22)$$

$$C_D = 0.275 + 0.00610 * \mathrm{A} + 31.3 * \mathrm{B} + 6.79 * \mathrm{C} - 1.21 * \mathrm{D} \quad (23)$$

where A, B, C, and D denoted angle, length, thickness, and position by percentage, respectively, while C_L and C_D were dependent and A, B, C, and D were independent variables. It should be noted that the corresponding levels of each factor previously determined in Table 1 were included in Eqs. (22–23).

In the confirmation test, the C_L and C_D were divided into two as testing and training. While there were 16 numerical tests in this study, 12 of them were used for training data of RA and the remaining 4 were used for testing data of RA. The empirical Eqs. (21–22) using the training data for the prediction of the C_L and C_D by RA were attained. Moreover, the testing data for the confirmation tests with attained empirical Eqs. (21–22) were carried out.

The comparison of testing and training data in terms of numerical and predicted C_L and C_D results is displayed in Fig. 9. The results were similar between the numerical and the predicted C_L and C_D for both training and test data. The C_L and C_D gained from numerical, RA training and RA testing, are presented in Fig. 10. While consistent

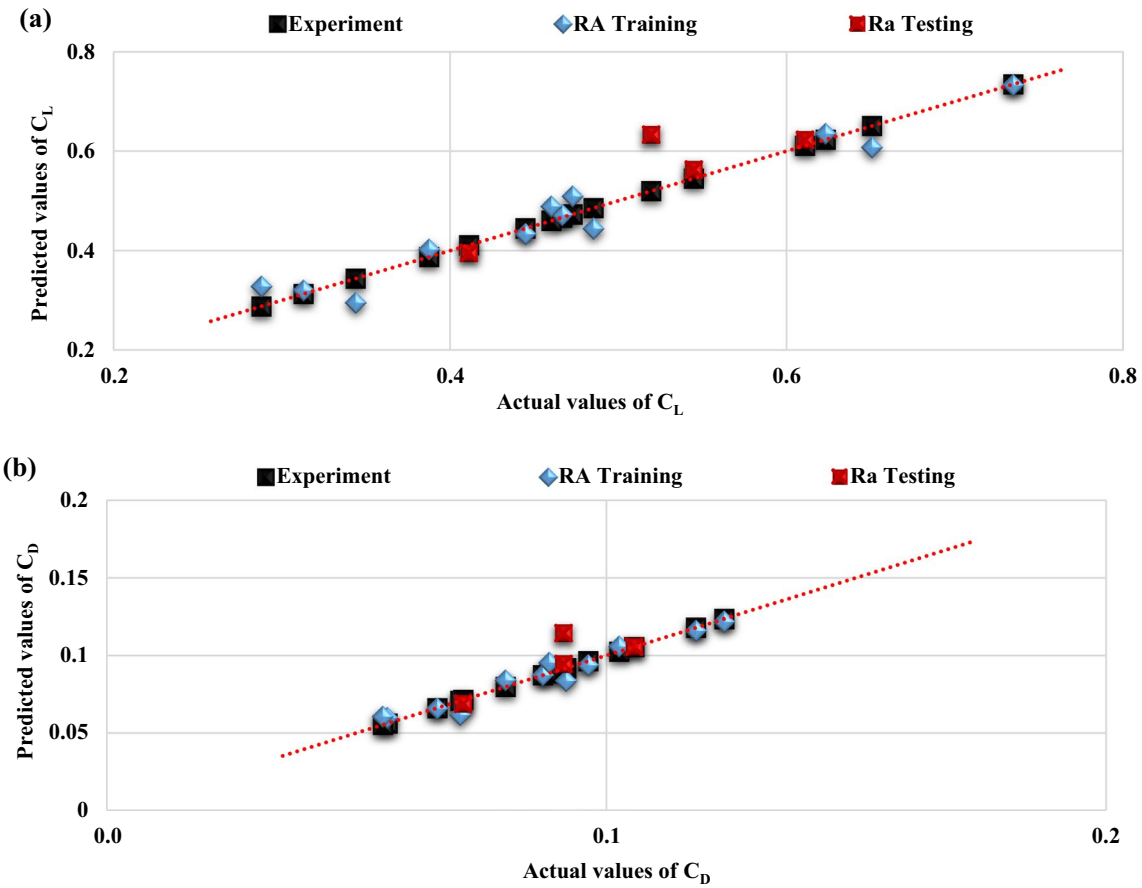


Fig. 9 Comparison of predicted and actual values of regression and numerical analyses for the **a** C_L and **b** C_D

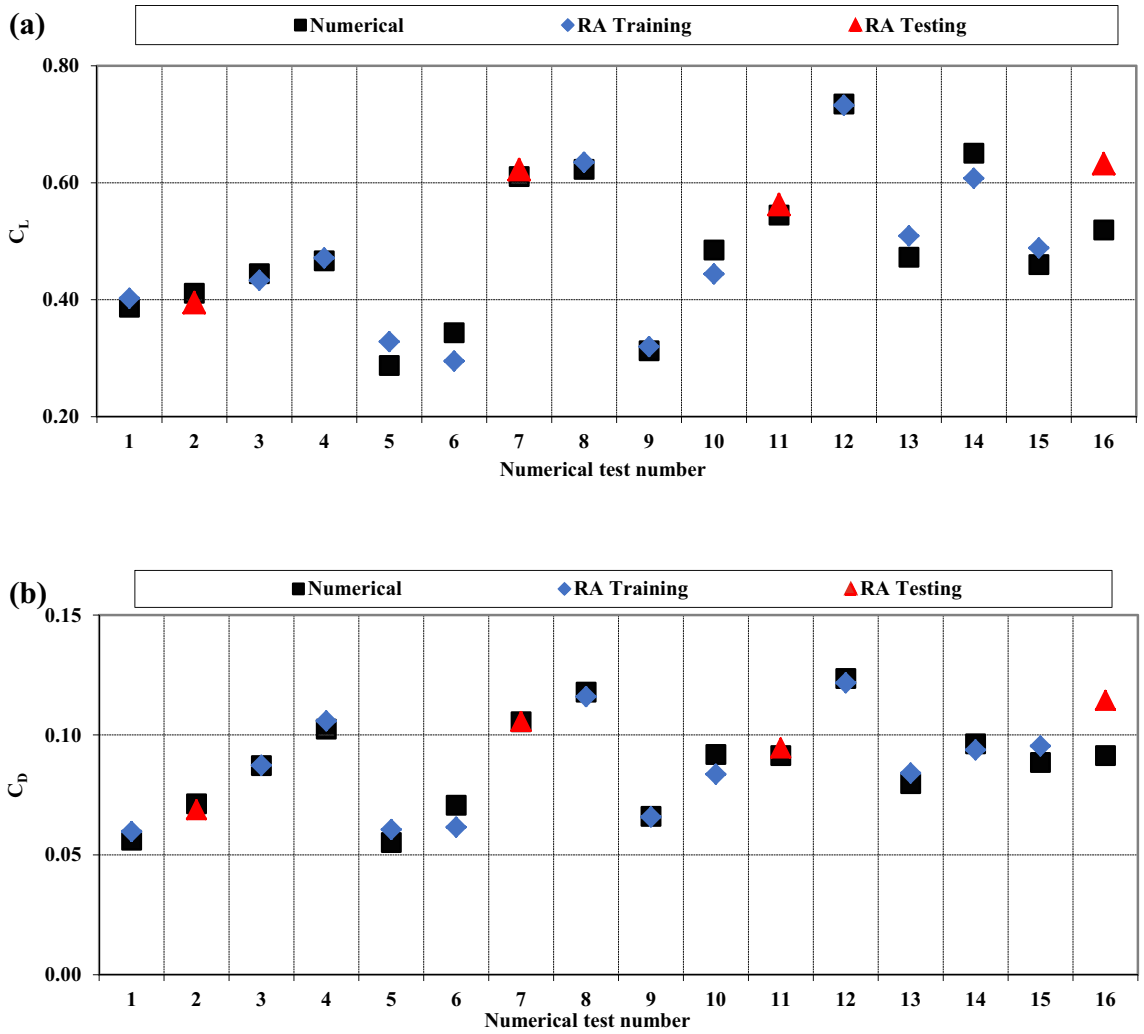


Fig. 10 Comparison of numerical and predicted results for **a** C_L and **b** C_D

data were obtained for almost all the results, only 2–3 numerical results indicated small deviations. The acquired RA models were demonstrated as an applicable and efficient way for the prediction of flap optimization in airfoils. The regression method and predictive modeling consist of two stages called testing and training. As a result of these stages, certain deviations occur between the estimated value and the actual value. Statistical analyses such as coefficient of determination (R^2) and amount of statistical error (RMSE) were used to determine the rate of this deviation. As can be seen in Eqs. (24–25), R^2 and RMSE can be calculated as below [51]:

$$R^2 = 1 - \left(\frac{\sum_{i=1}^{N} \left(t_i - o_i\right)^2}{\sum_{i=1}^{N} o_i^2} \right) \tag{24}$$

Table 8 Statistical results of training and testing data for aerodynamic performance

	Lift coefficient (C_L)		Drag coefficient (C_D)	
	RMSE	R^2	RMSE	R^2
Training data	0.002186	0.982489	0.03380	0.976941
Testing data	0.008534	0.956829	0.016645	0.919907

$$RMSE = \left(\frac{\sum_{i=1}^{N} \left(t_i - o_i\right)^2}{\sum_{i=1}^{N} o_i^2} \right)^2 \tag{25}$$

The accurate control of equation obtained with regression method is statistically shown in Table 8. R^2 data of

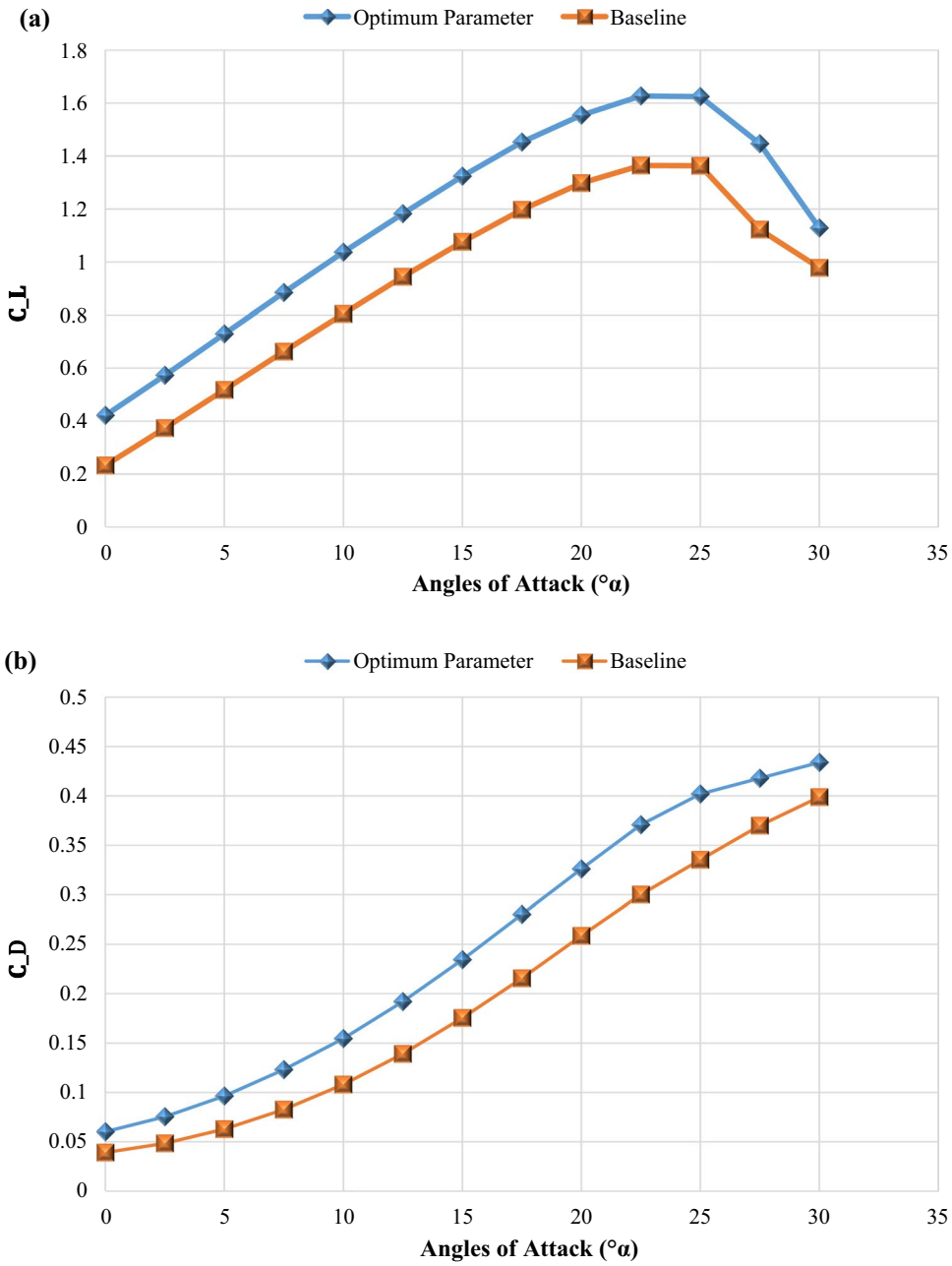


Fig. 11 Baseline and the optimum parameters ($\alpha = 75°$; $\Delta h = 1.5\%c$; $\Delta t = 2\%c$; $\Delta x = 0\%c$) comparison as **a** C_L and **b** C_D at various angles of attack as graph

both C_L and C_D attain with RA are calculated as 0.982489 and 0.976941. In addition, the RMSE values of C_L and C_D from RA were obtained as 0.002186 and 0.03380, respectively. Finally, both R^2 and RMSE data obtained by numerical result and RA indicate that γ_1 for aerodynamic performance is pretty reliable.

3.7 Aerodynamic investigation of the blade model

Until this section, the most effective blade model has been determined within the framework of the γ_1 approach. The determined model with optimum parameters ($\alpha = 75°$; $\Delta h = 1.5\%c$; $\Delta t = 2\%c$; $\Delta x = 0\%c$) was compared and evaluated with the baseline in terms of aerodynamic performance. In the optimization process, the C_L and C_D of the optimum parameters and the baseline, with the range 2.5°, between 0° and 30° angle of attack were numerically analyzed as displayed in Fig. 11. It was observed that the stall angle and C_L of the optimum parameters model were 22.5° and 1.67, respectively, while it was 25° and 1.32 on the baseline model parameters. It has been determined that the optimum parameter improves the maximum stall performance by 27%. In the region up to the stall, it was seen that both models acted with a similar slope by terms of C_L. In fact, the difference at 0° was maintained until the stall. After the stall, however, there was a sharper decrease at optimum

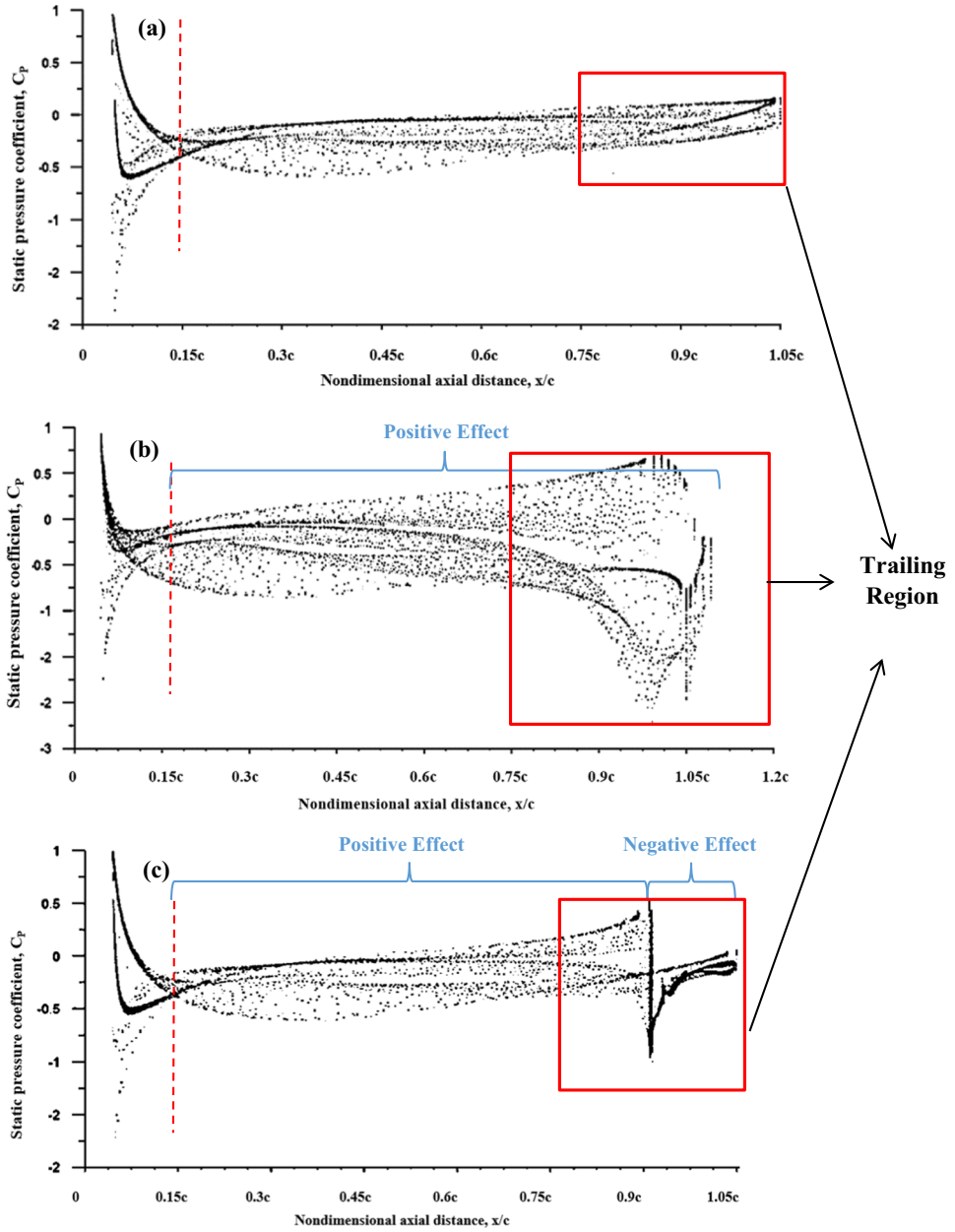


Fig. 12 The pressure coefficient graphs of **a** baseline **b** optimum parameters ($\alpha = 75°$; $\Delta h = 1.5\%c$; $\Delta t = 2\%c$; $\Delta x = 0\%c$) and **c** $\alpha = 90°$; $\Delta h = 6\%c$; $\Delta t = 4\%c$; $\Delta x = 18\%c$ (See Table 3: test no 4)

parameters as C_L compared to the baseline. The smallest difference between C_D of baseline and optimum parameters was attain at 0°, while the range between both blades was increased linearly at the high attack of angle. The positive effect of the flap after the stall for C_L was limited. However, at each stage of the angle of attack, the positive effect of the GF integrated into the straight airfoil as the C_L performance was clearly seen.

Figure 12 indicates that C_P (static pressure distribution) values across all surfaces of baseline, optimum parameters and test number "4" (see Table 2) at 0° angle of attack. The C_P is the main factor in the formation of the C_L. The degree of effect of the GF on C_P was investigated at different locations of the airfoil. In Fig. 12, the C_P of all models was similar in the leading-edge region ($0 \leq x \leq 0.15c$). It has been noticed that the C_P performance of the optimum parameters significantly was improved in the region from 0.15c to the trailing edge region compared to the baseline. In the trailing edge, the difference between the C_P of baseline and optimum parameters reached the supreme level due to the GF being in this region. As the perpendicular line at 0.9c in test number "4" has occurred due to it has the lowest C_L among orthogonal arrays. The sharp decrease of pressure difference at test number "4" prevented the formation of the lift force in the region between 0.9–1.05c. Briefly, in Fig. 12, it was observed that correctly at position and dimension, GF significantly increases the C_P in almost all the blade, except for a small part of the leading edge. In this case, it was concluded

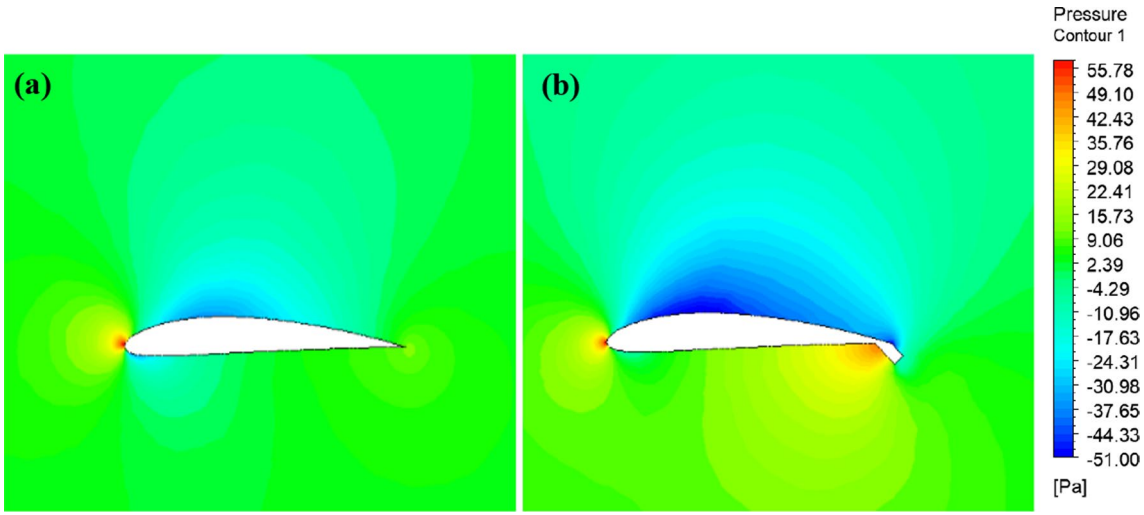


Fig. 13 Velocity contour for **a** baseline and **b** optimum parameters ($\alpha = 75°$; $\Delta h = 1.5\%$c; $\Delta t = 2\%$c; $\Delta x = 0\%$c) at 0° attack of angle

that the GF improved the C_P, not only in the trailing edge region but also in other regions. Figure 13 indicates that static pressure contours across all surfaces of baseline and optimum parameters at 0° angle of attack. While there was a very low pressure (dark blue color) area on the entire upper surface of the optimum parameters, it was limited in the baseline. On contrast, high-pressure (red color) areas were formed on the lower surface of the optimum parameters due to the tab geometry of the flap. The large pressure difference on the lower and upper surfaces of the blade at optimum parameters causes higher lift than the baseline, which supports Fig. 11. When evaluated in terms of aerodynamics, the GF structure, which was optimally integrated into the airfoil, has led to the formation of a vorticity region on the upper surface of the airfoil and furthermore a high-pressure difference in the trailing edge, and as a consequence of these two conditions, the lift performance has improved.

4 Conclusion

In this paper, the optimization of GF parameters on an aerodynamic process by using the Taguchi based on grey relational analysis approach was performed. The main results were as follows:

- The C_L and C_D of the baseline at 0° angle of attack were numerically obtained as 0.233 and 0.04.
- The optimum levels for angle, length, thickness, and position by γ_1 were determined at 75°, 1.5%c, 2%c, and 0%c, respectively. The percent of improvement γ_1 was enhanced 35.62% compared to the baseline.
- According to ANOVA results, the most significant parameter of the GF in terms of its effect on aerodynamic performance was the position, having a percentage contribution of 37.62%, while the angle was the least significant factor, having a percentage contribution of only 3.06%.
- R^2 obtained for confirmations of Regression analysis was shown 0.9568 and 0.9199, respectively, at C_L and C_D.
- The GRA method was an efficient and effective tool to optimize the airfoil aerodynamic performance over the GF in aerodynamic studies. Empirical equations of the aerodynamic performance were developed by multivariable RA, and the RA empirical equations showed a good congruence with numerical experiment results in the confirmation test.
- While the GF integrated on the airfoil before the stall has a significant effect on aerodynamic performance, its effect was limited after the stall.
- When examined *C*p graph, addition of GF to blades has been enhanced C_L not only at the trailing edge but also on all surfaces.
- The aerodynamic performance of the wind turbine blade with the gurney obtained using (by) the optimal γ_1 (high C_L; low C_D) has significantly improved compared to the straight blade. This shows the widespread use of optimal gurney flaps in wind turbines.

References

1. Panwar NL, Kaushik SC, Kothari S (2011) Role of renewable energy sources in environmental protection: a review. Renew Sustain Energy Rev 15:1513–1524. https://doi.org/10.1016/j.rser.2010.11.037

2. Hansen KL, Kelso RM, Dally BB (2011) Performance variations of leading-edge tubercles for distinct airfoil profiles. AIAA J 49:185–194. https://doi.org/10.2514/1.J050631
3. Zhang MM, Wang GF, Xu JZ (2014) Experimental study of flow separation control on a low-Re airfoil using leading-edge protuberance method. Exp Fluids 55:1710. https://doi.org/10.1007/s00348-014-1710-z
4. Shukla V, Kaviti AK (2017) Performance evaluation of profile modifications on straight-bladed vertical axis wind turbine by energy and Spalart Allmaras models. Energy 126:766–795. https://doi.org/10.1016/j.energy.2017.03.071
5. Ismail MF, Vijayaraghavan K (2015) The effects of aerofoil profile modification on a vertical axis wind turbine performance. Energy 80:20–31. https://doi.org/10.1016/j.energy.2014.11.034
6. Tanurun HE, Acır A (2019) The Numeric analysis of tubercle effect on modified NACA-0015 airfoil. J Polytech 22:185–195. https://doi.org/10.2339/politeknik.391800
7. Liebeck RH (1978) Design of subsonic airfoils for high lift. J Aircr 15:547–561. https://doi.org/10.2514/3.58406
8. Storms BL, Jang CS (1994) Lift enhancement of an airfoil using a gurney flap and vortex generators. J Aircr 31:542–547. https://doi.org/10.2514/3.46528
9. Li YJ, Wang J, Zhang P (2003) Influences of mounting angles and locations on the effects of Gurney flaps. J Aircr 40(3):494–498. https://doi.org/10.2514/2.3144
10. Meyer R, Hage W, Bechert DW et al (2006) Drag reduction on gurney flaps by three-dimensional modifications. J Aircr 43:132–140. https://doi.org/10.2514/1.14294
11. Zhu H, Hao W, Li C, Ding Q (2019) Numerical study of effect of solidity on vertical axis wind turbine with gurney flap. J Wind Eng Ind Aerodyn 186:17–31. https://doi.org/10.1016/j.jweia.2018.12.016
12. Zhang Y, Ramdoss V, Saleem Z et al (2019) Effects of root gurney flaps on the aerodynamic performance of a horizontal axis wind turbine. Energy 187:115955. https://doi.org/10.1016/j.energy.2019.115955
13. Fatahian E, Nichkoohi AL, Salarian H, Khaleghinia J (2019) Comparative study of flow separation control using suction and blowing over an airfoil with/without flap. In: sadhana-academy proceedings in engineering sciences 44(220):1–19. https://doi.org/10.1007/s12046-019-1205-y
14. Kumar PM, Samad A (2019) Introducing gurney flap to wells turbine blade and performance analysis with OpenFOAM. Ocean Engineering 187:106212. https://doi.org/10.1016/j.oceaneng.2019.106212
15. Saenz-Aguirre A, Fernandez-Gamiz U, Zulueta E et al (2019) Optimal wind turbine operation by artificial neural network-based active gurney flap flow control. Sustainability 11:1–17. https://doi.org/10.3390/su11102809
16. Yang J, Yang H, Zhu W et al (2020) Experimental study on aerodynamic characteristics of a gurney flap on a wind turbine airfoil under high turbulent flow condition. Appl Sci 10:1–21. https://doi.org/10.3390/app10207258
17. Fatahian E, Nichkoohi AL, Salarian H, Khaleghinia J (2020) Effects of the hinge position and suction on flow separation and aerodynamic performance of the NACA 0012 airfoil. J Braz Soc Mech Sci Eng 42:1–14. https://doi.org/10.1007/s40430-020-2170-4
18. Ni L, Miao W, Li C, Liu Q (2021) Impacts of gurney flap and solidity on the aerodynamic performance of vertical axis wind turbines in array configurations. Energy 215:118895. https://doi.org/10.1016/j.energy.2020.118915
19. Zhu H, Hao W, Li C et al (2021) Effect of geometric parameters of gurney flap on performance enhancement of straight-bladed vertical axis wind turbine. Renew Energy 165:464–480. https://doi.org/10.1016/j.renene.2020.11.027
20. Sun G, Wang Y, Xie Y et al (2021) Research on the effect of a movable gurney flap on energy extraction of oscillating hydrofoil. Energy. https://doi.org/10.1016/j.energy.2021.120206
21. Wilcox DC (1998) Turbulence modeling for CFD. DCW Industries, Inc., La Canada, California
22. Alaimo A, Esposito A, Messineo A, Orlando C, Tumino D (2015) 3D CFD analysis of a vertical axis wind turbine. Energies 8:3013–3033. https://doi.org/10.3390/en8043013
23. Mohamed OS, Ibrahim AA, Etman AK, Abdelfatah AA, Elbaz AMR (2020) Numerical investigation of Darrieus wind turbine with slotted airfoil blades. Energy Convers Manag X 5:100026. https://doi.org/10.1016/j.ecmx.2019.100026
24. Mohamed OS, Ibrahim AA, Etman AK et al (2020) Numerical investigation of Darrieus wind turbine with slotted airfoil blades. Energy Convers Manag 5:100026. https://doi.org/10.1016/j.ecmx.2019.100026
25. Obeid S, Jha R, Ahmadi G (2017) RANS Simulations of aerodynamic performance of NACA 0015 flapped airfoil. Fluids 2(1):1–27. https://doi.org/10.3390/fluids2010002
26. Mohamed MH, Ali AM, Hafiz AA (2015) CFD analysis for H-rotor Darrieus turbine as a low speed wind energy converter. Eng Sci Technol Int J 18:1–13
27. Kaya AF, Acir A, Tanurun HE (2020) Numerical investigation of radius dependent solidity effect on H-type vertical axis wind turbines. J Polytechnic. https://doi.org/10.2339/politeknik.799767
28. Lin CL (2004) Use of the Taguchi method and grey relational analysis to optimize turning operations with multiple performance characteristics. Mater Manuf Processes 19:209–220. https://doi.org/10.1081/AMP-120029852
29. Acır A, Canlı ME, Ata İ, Çakıroğlu R (2017) Parametric optimization of energy and exergy analyses of a novel solar air heater with grey relational analysis. Appl Therm Eng 122:330–338. https://doi.org/10.1016/j.applthermaleng.2017.05.018
30. Fu C, Zheng J, Zhao J, Xu W (2001) Application of grey relational analysis for corrosion failure of oil tubes. Corros Sci 43:881–889. https://doi.org/10.1016/S0010-938X(00)00089-5
31. Kuo Y, Yang T, Huang GW (2008) The use of grey relational analysis in solving multiple attribute decision-making problems. Comput Ind Eng 55(1):80–93. https://doi.org/10.1016/j.cie.2007.12.002
32. Ghani JA, Choudhury IA, Hassan HH (2004) Application of Taguchi method in the optimization of end milling parameters. J Mater Process Technol 145:84–92. https://doi.org/10.1016/S0924-0136(03)00865-3
33. Sahin İ, Acir A (2015) Numerical and experimental investigations of lift and drag performances of NACA 0015 wind turbine airfoil. Int J Mater Manuf 3:22–25. https://doi.org/10.7763/ijmmm.2015.v3.159
34. Singhal A, Castañeda D, Webb N, Samimy M (2018) Control of dynamic stall over a NACA 0015 airfoil using plasma actuators. AIAA J 56:78–89. https://doi.org/10.2514/1.J056071
35. Tanurun HE, Ata İ, Canlı ME, Acır A (2019) Numerical and experimental investigation of NACA-0018 wind turbine aerofoil model performance for different aspect ratios. J Polytech 23:371–381. https://doi.org/10.2339/politeknik.500043
36. Rogowski K, Hansen MOL, Bangga G (2020) Performance analysis of a H-Darrieus wind turbine for a series of 4-digit NACA airfoils. Energies 13(12):1–28. https://doi.org/10.3390/en13123196
37. Yu H, Zheng J (2020) Numerical investigation of control of dynamic stall over a NACA0015 airfoil using dielectric barrier discharge plasma actuators. Phys Fluids 32:035103. https://doi.org/10.1063/1.5142465
38. Tanurun HE, Acır A (2022) Investigation of the hydrogen production potential of the H-Darrieus turbines combined with various wind-lens. Int J Hydrogen Energy 47(55):23118–23138. https://doi.org/10.1016/j.ijhydene.2022.04.196

39. Meana-Fernández A, Oro JF, Díaz KA, Velarde-Suárez S (2019) Turbulence-model comparison for aerodynamic-performance prediction of a typical vertical-axis wind-turbine airfoil. Energies 12(3):488. https://doi.org/10.3390/en12030488
40. Michal T, Joshua K, Kamenetskiy D, Galbraith M, Ursachi C, Park MA, Anderson WK, Alauzet F, Loseille A (2021) Comparing unstructured adaptive mesh solutions for the high lift common research airfoil. AIAA J 59(9):3566–3584. https://doi.org/10.2514/1.J060088
41. Sener MZ, Aksu E (2022) The numerical investigation of the rotation speed and Reynolds number variations of a NACA 0012 airfoil. Ocean Eng 249:110899
42. Wong KH, Chong WT, Sukiman NL et al (2018) Experimental and simulation investigation into the effects of a flat plate deflector on vertical axis wind turbine. Energy Convers Manage 160:109–125. https://doi.org/10.1016/j.enconman.2018.01.029
43. Lam HF, Peng HY (2016) Study of wake characteristics of a vertical axis wind turbine by two- and three-dimensional computational fluid dynamics simulations. Renew Energy 90:386–398. https://doi.org/10.1016/j.renene.2016.01.011
44. Tanurun HE, Akin A, Acir A (2021) Numerical investigation of rib structure effects on performance of wind turbines. J Polytech 24(3):1219–1226. https://doi.org/10.2339/politeknik.845804
45. Bouremel Y, Li JM, Zhao Z, Debiasi M (2013) Effects of AC dielectric barrier discharge plasma actuator location on flow separation and airfoil performance. In: 7th Asian-Pacific conference on aerospace technology and science (APCATS), Taiwan. pp 270–78
46. Tebbiche H, Boutoudj MS (2015) Flow passive control on the naca airfoils experimental and numerical study. In: VI international conference on computational methods for coupled problems in science and engineering (CIMNE) Venice, Italy
47. Jukes TN, Segawa T, Furutani H (2013) Flow control on a NACA 4418 using dielectric-barrier-discharge vortex generators. AIAA J 51:452–464. https://doi.org/10.2514/1.J051852
48. Ostowari C, Naik D (1985) Post stall studies of untwisted varying aspect ratio blades with NACA 44XX series airfoil sections—Part II". Wind Eng 9(3):149–164
49. Sekimoto S, Asada K, Usami T, et al (2011) Experimental study of effects of frequency for burst wave on DBD plasma actuator for separation control. In: 41st AIAA fluid dynamics conference and exhibit. Hawai, ABD, pp 1–13
50. Yang WH, Tarng YS (1998) Design optimization of cutting parameters for turning operations based on the Taguchi method. J Mater Process Technol 84:122–129. https://doi.org/10.1016/S0924-0136(98)00079-X
51. Çakıroğlu R (2022) Analysis of Ranque–Hilsch vortex tube cooling performance in respect of cutting temperature, resultant cutting force and chip morphology in turning of becu alloy. J Braz Soc Mech Sci Eng 44(371):1–18. https://doi.org/10.1007/s40430-022-03689-3

Publisher's Note Springer Nature remains neutral with regard to jurisdictional claims in published maps and institutional affiliations.

Springer Nature or its licensor (e.g. a society or other partner) holds exclusive rights to this article under a publishing agreement with the author(s) or other rightsholder(s); author self-archiving of the accepted manuscript version of this article is solely governed by the terms of such publishing agreement and applicable law.